

Implications on crustal structure from the South Finland Coastal (SOFIC) deep seismic sounding profile



TIMO TIIRA^{1*}, TOMASZ JANIK², TONI VEIKKOLAINEN¹,
KARI KOMMINAHO¹, TYMON SKRZYNIK², SAKARI VÄKEVÄ³
AND AKU HEINONEN⁴

¹ *Institute of Seismology, Department of Geosciences and Geography, University of Helsinki, P.O. Box 68, 00014 Helsinki, Finland.*

² *Institute of Geophysics, Polish Academy of Sciences, Księcia Janusza 64, 01-452 Warsaw, Poland.*

³ *Data and Information Centre, Finnish Environment Institute, Latokartanonkaari 11, 00790 Helsinki, Finland.*

⁴ *Geological Survey of Finland, P.O. Box 96, 02151 Espoo, Finland.*

Abstract

We present results from a deep seismic sounding (DSS) experiment carried out along the southern coast of Finland in summer 2015. Data used in the survey derived from industrial blasts recorded by temporary project stations and permanent network stations. The western 220 km part of the 450 km long Southern Finland Coastal (SOFIC) profile runs along the Uusimaa belt (UB) in the 1.7–1.9 Ga Southern Finland subprovince (SFS) of the Svecofennian domain, while the 170 km part in the east crosses the 1.62–1.65 Ga Wiborg rapakivi batholith (WRB). The farthest 60 km cross a geologically diverse area consisting of supracrustal rocks and granitoids of the Saimaa area (SA), an eastern extension of the SFS. Our results show that the Moho boundary depth varies significantly, from ca. 52–54 km below UB to 40–45 km below WRB. All three crustal layers (upper, middle, and lower) have their maximum depth in the contact zone between UB and the WRB. Below WRB, a lower crust with V_p ~6.7–6.9 km/s is observed. High velocity lower crust was observed below UB (V_p ~7.2 km/s) and possibly below SA (V_p ~7.35 km/s). The modelling was based on ray tracing, using the extrapolation of seismic wave arrival times with the help of travel times predicted from a one-dimensional velocity model. The resulting two-dimensional velocity model partly relies on data from the intersecting DSS profiles and supports previous observations of the lithospheric structure of southeastern Fennoscandia.

Keywords: seismology, Moho, reflection, profile, crust, lithosphere, Fennoscandia, Precambrian

* Corresponding author (e-mail: timo.tiira@helsinki.fi)

Editorial handling: Suvi Heinonen (e-mail: suvi.heinonen@gtk.fi)

1. Introduction

The South-Finland Coast (SOFIC) Deep Seismic Sounding (DSS) profile crosses four previous DSS lines: BALTIC (Luosto et al. 1990; Janik 2010), FENNIA (Janik et al. 2007), FIRE2a (Kukkonen & Lahtinen 2006; Korja & Heikkinen 2008) and KOKKY (Tiira et al. 2020). SOFIC is based on an experiment, which resembles the Kokkola–Kymi (KOKKY) profile and was initiated to increase knowledge of the lithospheric structure in an area where industrial blasts are common due to construction and quarry activities.

Except for its western coast, the southern-

central Finland is relatively well covered by structural seismology profiles (Figure 1). However, most experiments have been carried out along NE–SW to N–S directed lines as determined by the previously assumed E–W crustal architecture produced during the Paleoproterozoic Svecofennian orogeny. Although the KOKKY profile in NW–SE direction was an improvement to the situation, no surveys in W–E direction have previously been carried out in southern Finland. Thus, the SOFIC profile is the first of its kind. It begins from Kasnäs on the coast of Archipelago Sea and ends at the western coast of Lake Ladoga in the northern part of the Karelian Isthmus.

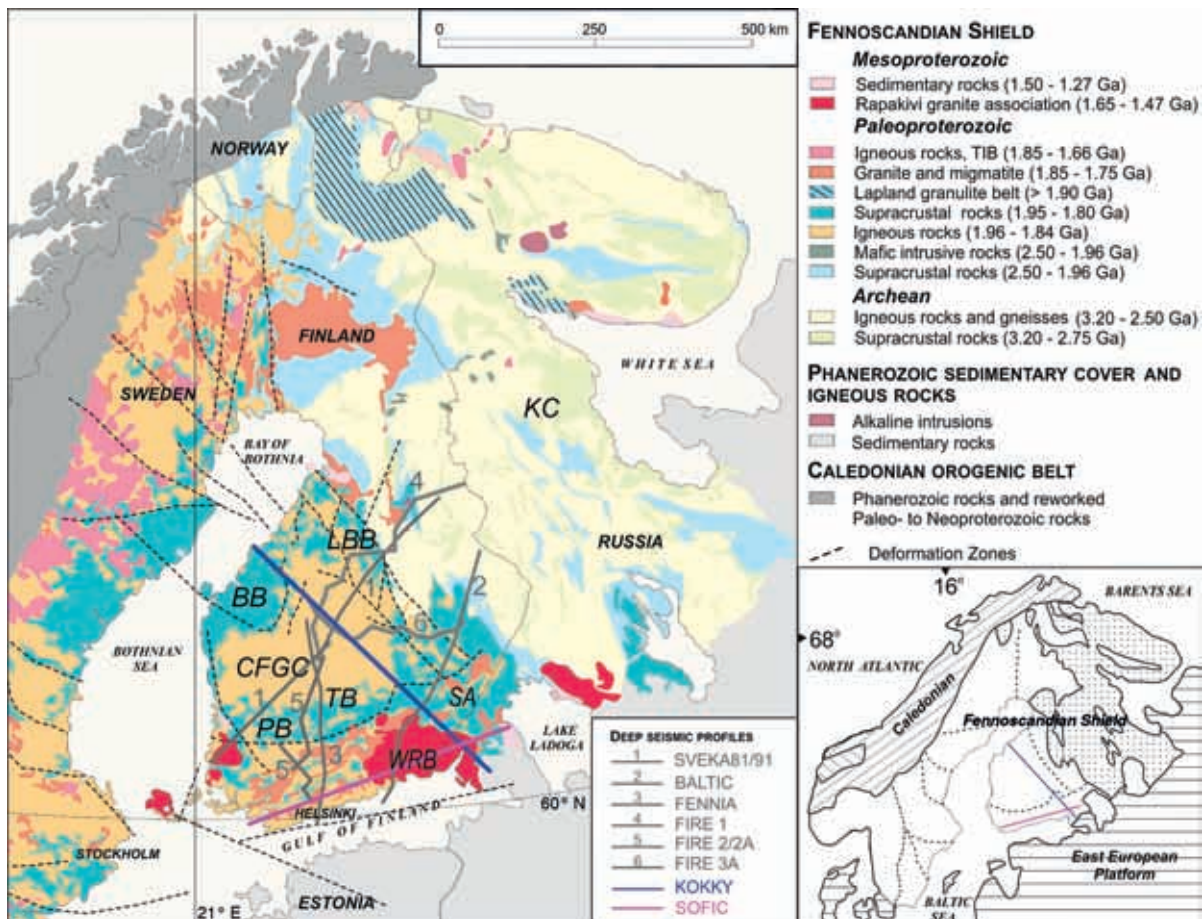


Figure 1. Geological map of Fennoscandian Shield and adjacent areas. SOFIC and previous deep seismic profiles of southern and central Finland are shown. Large map: BB = Bothnian Belt, CFGC = Central Finland Granitoid Complex, HB = Häme Belt, LBB = Ladoga-Bothnia Boundary, PB = Pirkanmaa Belt, TB = Tampere Belt, SA = Saimaa Area, UB = Uusimaa Belt, WRB = Wiborg Rapakivi Batholith. Small map: CFS = Central Finland Subprovince, SFS = Southern Finland Subprovince. Modified after Lahtinen et al. (2005).

Geologically the SOFIC profile runs for its entirety within the Southern Finland subprovince (SFS) of the Paleoproterozoic Svecofennian domain (Nironen 2017). The SFS comprises two discrete allochthonous, dominantly supracrustal east-northeast striking belts: The Uusimaa belt (UB) in the south and the Häme belt (HB) in the north, which are suggested to have amalgamated onto the continental margin towards present day north at approximately 1.89–1.86 Ga during the last accretionary stages of the Svecofennian orogeny (Lahtinen et al. 2005; Nironen 2017). The SFS corresponds broadly to the arc complex of southern Finland (ACSF) in earlier interpretations of the regional crustal architecture (e.g. Kähkönen 2005). In the most recent interpretation (Nironen 2017) the relatively poorly known Saimaa area (SA) in the easternmost part of the SOFIC profile has been affiliated with the SFS. In earlier models (e.g. Kähkönen 2005) it has been considered to share a broadly similar geotectonic history with the Pirkanmaa belt in the arc complex of western Finland (ACWF, now called the central Finland subprovince, CFS, of the Svecofennian domain). After the accretionary stages the (ca. 1.92–1.86 Ga) syn-orogenic supracrustal and intrusive rocks of SFS were first intruded by the late- to post-orogenic (1.85–1.82 Ga) alkali feldspar granites of the southern Finland granite suite (see Kurhila 2011 and references therein), most likely related to the extensional collapse of the accretionary orogen (e.g. Nironen 2017). Considerably later, between 1.65–1.52 Ga, the entire SFS was affected by the anorogenic rapakivi suite magmatism (Rämö & Haapala, 2005; Rämö et al. 2014; Heinonen et al. 2016, 2017). The majority of the eastern part of the SOFIC profile runs across the largest intrusion of the rapakivi suite in southeastern Finland – the ca. 1.63 Ga Wiborg rapakivi batholith (WRB). In its far eastern end, the profile meets Neo-Mesoproterozoic rocks of the basin structure of Lake Ladoga.

Due to the multi-stage Proterozoic geological and tectonic history, the surface geology along SOFIC profile consists of a mixture of different kinds of rock types but can roughly be separated

into three geologically and structurally relatively coherent domains: the western SFS (Uusimaa belt), WRB (Wiborg rapakivi batholith), and the eastern SFS (Saimaa area). In the western part of the SFS 1.85–1.75 Ga granites and migmatites, various 1.96–1.84 Ga igneous rocks, and 1.95–1.80 Ga supracrustal rock types (granodiorites, microcline granites, paragneisses, quartz feldspar gneisses, and amphibolites) all with large-scale E–W tectonic fabric and structural tendencies dominate. Within WRB, the surface geology comprises relatively homogeneous 1.65–1.62 Ga granitic rocks without any obvious tectonic or syn-intrusional structures (Rämö and Haapala 2005). In the eastern SFS, 1.95–1.80 Ga supracrustal rocks, 1.85–1.75 Ga granites and migmatites, and 1.50–1.27 Ga sedimentary rocks are present. In contrast to the western SFS with clear E–W fabric across much of the region, the eastern SFS has more varied structural features. The layered structure of Svecofennian crust has been demonstrated in several studies (Korja et al. 1993; Luosto 1997; Hyvönen et al. 2007), yet horizontal velocity variations are in favor of an assembly of several sub-blocks during the orogeny. The aim of the SOFIC profile was to probe the differences between Svecofennian and younger lithosphere in the southeastern part of the Fennoscandian shield area.

2. Data acquisition

SOFIC seismic data were gathered in a project in May–June 2015 along a 450 km profile. Data derive entirely from industrial and military blasts. The procedure was very similar to that used in the KOKKY survey, which was carried out in 2012–2013 on a 490 km line spanning from Central Ostrobothnia to the vicinity of Russian border in South Karelia (Tiira et al. 2020). The low cost and minimal license formalities are an advantage of this kind of project compared to regular wide-angle refraction and reflection (WARR) surveys with explosions produced only for the purpose of the DSS project.

The Institute of Seismology, University of Helsinki, gathered data in a summer campaign in 2015. Altogether 59 Data-Cube recorders and geophones were installed. Also, 44 Trimble Ref Tek 125 (Texan) portable seismic stations were installed close to the southern coast of Finland approximately following the national highway 7, so that every second station was a Data-Cube and every second was a Texan. However, the majority of Texan data were lost due to data corruption, and therefore only 7 of these stations could be used, leading to the average spacing of stations being double the planned, approximately 6 km. Additional data from stations of the Finnish National Seismic Network (FNSN; Veikkolainen et al. 2021) were used to improve the time and location accuracy of seismic events, and were also included for seismic modelling.

In total, 56 quarry blasts and other explosions were considered during the project for analysis, based on their proximity to the SOFIC profile. Altogether 46 of them passed the quality criteria, 41 of them from Finland and the rest from Russia. The shot locations were initially unknown but were resolved from the data of the temporary deployment, four stations of the permanent FNSN network (MVF, NUR, PVF, VJF) and one temporary FNSN station of the network densification of Kouvola area (KV1). For preliminary determination of locations, an ordinary least-squares method included in the HYP locator of SeisAn software (Havskov & Ottemoller 1999) was applied. For additional verification, the known locations of quarries and mines, aerial orthomosaics of the National Land Survey of Finland, as well as other digital maps were used. Events close to any open quarry, mine or construction site were associated with the known location. Because of the high location accuracy, over 1 km, it was possible to associate several shots reliably to the same site. The location accuracy was higher on the Finnish than on the Russian territory, because all stations were located in Finland. Notable shot locations in Finland involve sea blast sites in Örö, the Skräbböle

mine in Parainen, the construction site of the harbour in Inkoo, a quarry in Koivikko, Vantaa, a quarry in Järvenpää, a quarry in Rajavuori, Kotka, a quarry in Laapas, Luumäki, a quarry in Ruokosuo, Virolahti, and a quarry in Ihalainen, Lappeenranta. Seismic events from Russia could be associated to the quarries of Kamennogorsk, Kuznetshnoye and Vodrozhdenie. The farthest shots were from the vicinity of the coast of Lake Ladoga in the northern part of the Karelian Isthmus.

Estimation of origin times was done by extrapolation of station arrival times to past, using the predicted travel times to project stations and permanent stations in a way similar to that used for the KOKKY profile. The initial one-dimensional velocity model was that used in the routine analysis at the institute. In the model, the topmost layer (0–15 km) is mainly granitic and underlain by a mainly basaltic layer (15–40 km) above the mantle (Table 1). Geotool software of the Comprehensive Test-Ban Treaty Organization (CTBTO, <https://www.ctbto.org>) was used for manual picking of seismic events. Origin times were estimated once, by extrapolation of station arrivals backwards in time. Seismic stations in different azimuthal directions were used, assuming that the mean error of the origin time decreases by \sqrt{N} where N is the number of stations. The mean origin time for each source was calculated by subtraction of travel times estimated from the velocity model from arrival times of seismic phases. The acceptance criteria for the origin time were as follows: a standard error of the mean had to be less than 0.05 s and the minimum number of seismic phases used for location needed to be at least five. If the origin time did not pass the criteria, we dropped the event because it most likely had an inaccurate location.

Table 1. Seismic velocity model used at the Institute of Seismology, University of Helsinki.

Vp (km/s)	Vs (km/s)	Depth range
6.19	3.60	0–15 km
6.70	3.84	15–40 km
8.03	4.64	40 km →

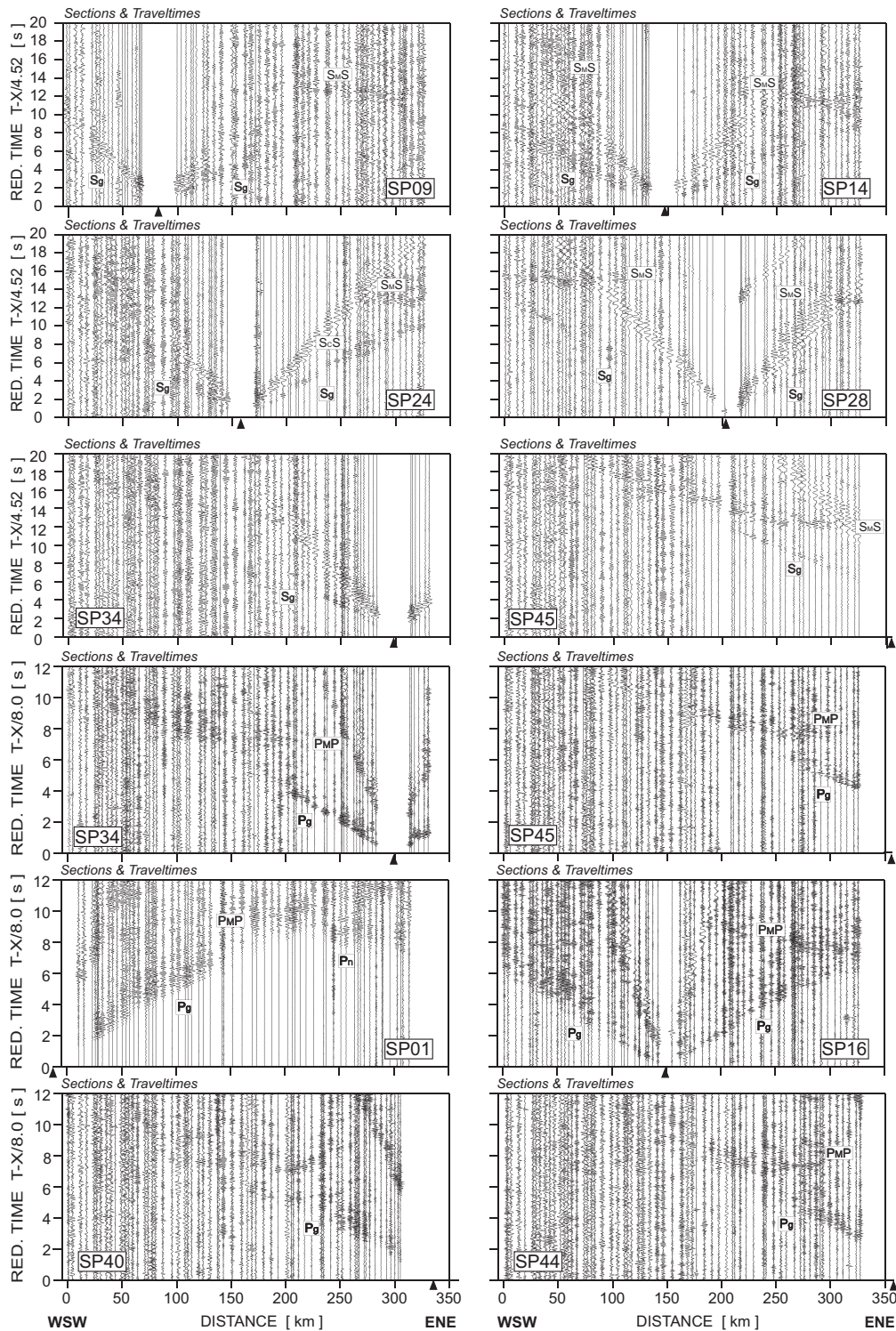


Figure 2. Examples of recorded seismic sections: (a) for P-wave (reduced velocity 8 km/s, filter 2–15 Hz) and (b) for S-wave (reduced velocity 4.52 km/s, filter 1–6 Hz) are illustrated in separate subplots of shots: 1, 16, 34, 40, 44, 45 and 9, 14, 24, 28, 34, 45, respectively. Abbreviations: P_g and S_g – P and S refractions from the upper and middle crystalline crust; P_cP – reflections from mid-crustal discontinuities, $P_M P$ and $S_M S$ – P and S waves reflected from the Moho boundary; P_n – refractions from the uppermost mantle.

Table 2. Details of shots used for construction of SOFIC profile. Shot numbers are not in time order.

Shot number	Latitude (degrees)	Longitude (degrees)	*Distance	**Offset	Date	Time in UTC
1	59.7160	22.2960	-15.88	21.2	01.06.2015	13:34:25.97
2	59.6907	22.2851	-15.82	23.0	01.06.2015	13:47:55.72
3	60.2894	22.2714	4.51	40.6	26.05.2015	10:57:10.94
4	60.2909	22.2714	4.57	40.8	04.06.2015	11:00:35.32
5	60.1779	23.1613	47.59	13.7	02.06.2015	12:14:18.23
6	60.4193	23.2784	61.90	37.2	27.05.2015	08:42:40.32
7	60.2402	23.4948	67.33	11.4	26.05.2015	11:41:58.21
8	60.0182	23.9329	83.31	16.3	04.06.2015	12:01:07.3
9	60.0183	23.9333	83.33	16.3	01.06.2015	11:58:55.30
10	60.1059	24.3602	108.93	13.8	02.06.2015	12:01:14.50
11	60.1052	24.3617	108.98	13.9	27.05.2015	11:31:32.80
12	60.2420	24.5280	123.79	3.1	28.05.2015	13:10:06.07
13	60.1627	24.7333	130.61	13.6	02.06.2015	18:10:21.23
14	60.4144	24.8266	143.40	11.9	27.05.2015	11:00:17.74
15	60.2990	24.9110	144.41	1.1	29.05.2015	08:07:54.70
16	60.3590	24.9120	146.21	4.7	26.05.2015	10:46:34.41
17	60.3629	24.9183	146.66	5.0	03.06.2015	10:57:36.94
18	60.3220	24.9420	147.19	1.6	25.05.2015	14:57:13.46
19	60.3683	24.9220	147.03	5.5	28.05.2015	10:44:19.82
20	60.2640	25.0800	123.82	8.0	28.05.2015	08:31:35.98
21	60.4320	25.1190	160.24	9.4	04.06.2015	15:03:54.10
22	60.4561	25.1071	160.24	12.1	27.05.2015	14:15:18.65
23	60.4557	25.1080	160.24	12.1	01.06.2015	14:36:58.03
24	60.4420	25.1170	160.24	10.5	25.05.2015	14:06:42.00
25	60.2940	25.5090	175.97	11.3	27.05.2015	14:19:41.05
26	60.2984	25.5309	177.27	11.1	04.06.2015	14:15:42.90
27	60.4930	25.9572	205.68	3.5	27.05.2015	10:26:12.39
28	60.5574	25.9231	205.76	10.9	02.06.2015	12:04:14.50
29	60.5006	26.8242	251.97	7.8	25.05.2015	10:35:11.44
30	60.4356	26.9137	252.77	9.8	28.05.2015	16:45:51.21
31	60.7640	27.0220	269.73	17.9	03.06.2015	12:18:57.68
32	60.6650	27.2940	281.44	3.6	25.05.2015	09:28:03.55
33	60.5519	27.6342	296.56	13.1	29.05.2015	08:15:11.19
34	60.5434	27.6920	299.36	14.8	27.05.2015	08:55:23.75
35	60.8309	27.8261	314.03	14.6	02.06.2015	06:46:34.87
36	60.8340	27.8483	315.28	14.7	05.06.2015	08:49:54.14
37	60.7100	27.9620	318.08	0.23	03.06.2015	09:06:00.95
38	60.8439	27.9192	319.29	14.8	02.06.2015	09:57:49.73
39	61.0335	28.1814	338.01	32.1	04.06.2015	10:33:29.14
40	61.0332	28.1821	338.04	32.1	28.05.2015	10:33:43.94
41	61.0060	28.1980	338.06	32.0	03.06.2015	10:33:30.48
42	60.8480	28.9734	375.24	2.3	31.05.2015	08:11:42.50
43	60.8416	28.9839	375.64	1.5	04.06.2015	08:14:57.06
44	60.9473	29.1811	388.64	10.7	29.05.2015	12:10:23.72
45	61.1330	29.8151	426.49	23.8	02.06.2015	18:07:25.82
46	61.1120	29.9125	431.15	20.4	03.06.2015	14:03:21.49

*Distance from the beginning of the profile line (km)

**Offset from the profile line (km)

The quality of each of the 46 registered seismic sections highly varied between sections for both P- and S-waves. The onsets were less distinct for S-wave than for P-wave data possibly due to the coupling between the soil and the geophone. Basic bandpass filtering was applied to the data, 2–15 Hz for P-wave and 1–6 Hz for S-wave seismic sections. Examples of shot recordings for P-wave and S-wave are shown in Figure 2, and accepted shot locations are listed in Table 2.

2.1. P- and S-waves

On most recorded sections, seismic phases corresponding to the first arrivals (P_g) are visible only to a distance of several dozen kilometres from the projected source point. Only on a minority of recorded sections (SP01–SP03, SP12–SP30), P_g arrivals are easily visible up to longer distances against the background of a relatively high level of noise. Apparent velocities in the range of 6.00–6.25 km/s reveal the crystalline basement and can

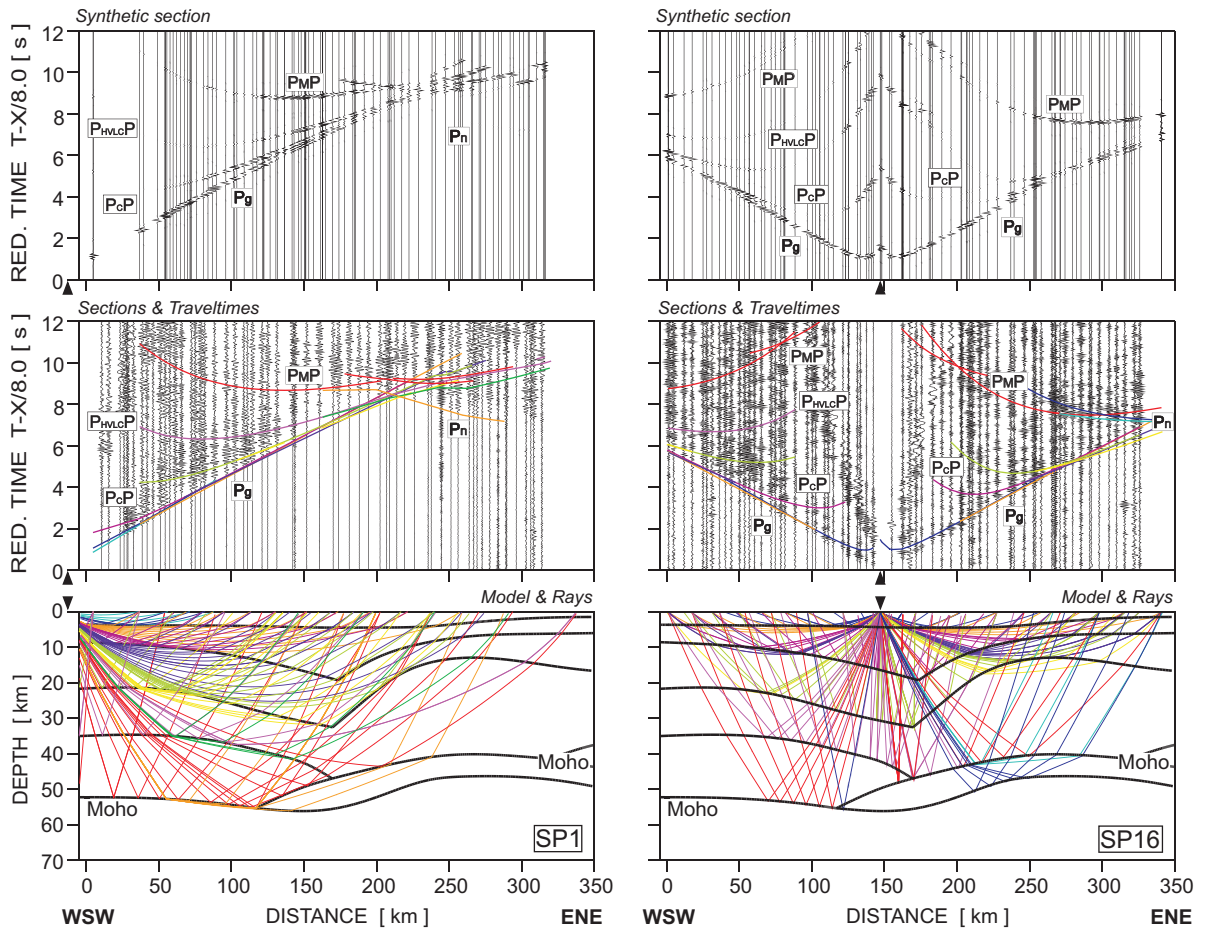


Figure 3. Examples of seismic modelling along the SOFIC profile, for P-wave arrivals of shots 1 and 16. Diagrams: synthetic seismograms derived by using the SEIS83 package (top); seismic record section (trace-normalized, vertical-component, 2–15 Hz band-pass filtered, reduction velocity of 8.0 km/s) of P-waves with theoretical travel times calculated using SEIS83 (middle); selected rays defining the prominent model interfaces (bottom). Abbreviations of seismic phases as in Figure 2 and P_{HVLC} P and S_{HVLC} S – P and S waves reflected from the top of the high velocity lower crust.

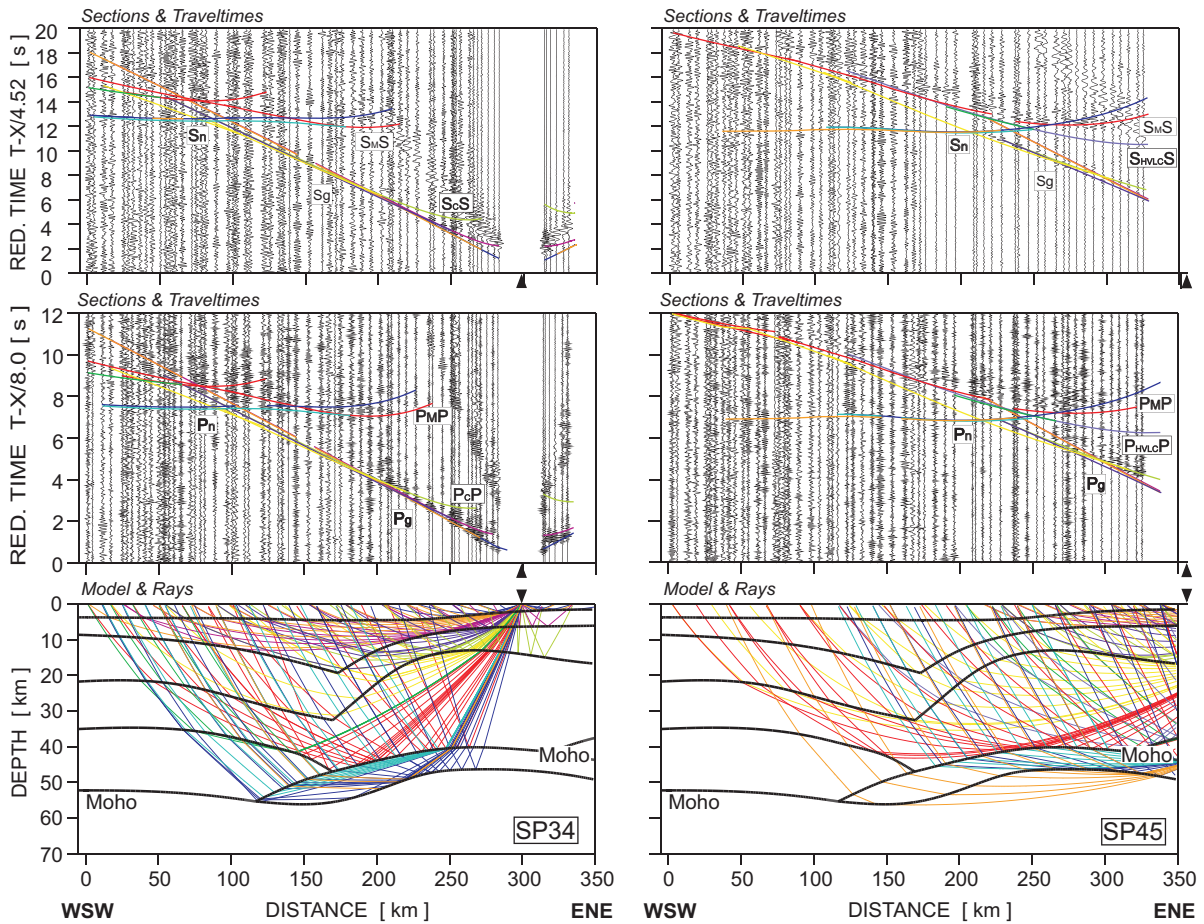


Figure 4. Examples of seismic modelling, for P- and S-wave arrivals of shots 34 and 45. Diagrams: seismic record section (trace-normalized, vertical-component, 2–15 Hz band-pass filtered, reduction velocity of 8.0 km/s) of P-waves with theoretical travel times (top); seismic record section (trace-normalized, vertical-component, 1–6 Hz band-pass filtered, reduction velocity of 4.52 km/s) of S-waves with theoretical travel times (middle); selected rays defining the prominent model interfaces (bottom). Abbreviations of seismic phases as in Figures 2 and 3.

be picked at approximately 200 km long offsets on only a few sections. The best quality of P_g arrivals was recorded on the section of SP01 (Figure 3). This section also showed a well-developed mantle phase refraction under Moho boundary (P_n) with a high apparent velocity > 9.2 km/s, distinguishable up to a distance of approximately 300 km. Only a few mid-crustal reflections (P_cP) are distinguishable (Figure 3). The Moho reflections ($P_M P$) are well visible on certain seismic sections (SP28, SP29, SP30, SP34, SP36, SP40, SP43–45).

The quality of the S-wave record sections is only slightly inferior compared to P-wave sections. The

strongest shots generated well visible S_g and $S_M S$ signals, and only few mid-crustal reflections ($S_c S$), and not upper mantle arrivals (Figure 4).

2.2. Ray tracing modelling

Due to the limited coverage of observations on the SOFIC profile, it is difficult to prepare a data-driven two-dimensional model for it without additional constraints from earlier seismic studies. However, the acquired data can be used to build on an initial velocity model, created using data collected on earlier

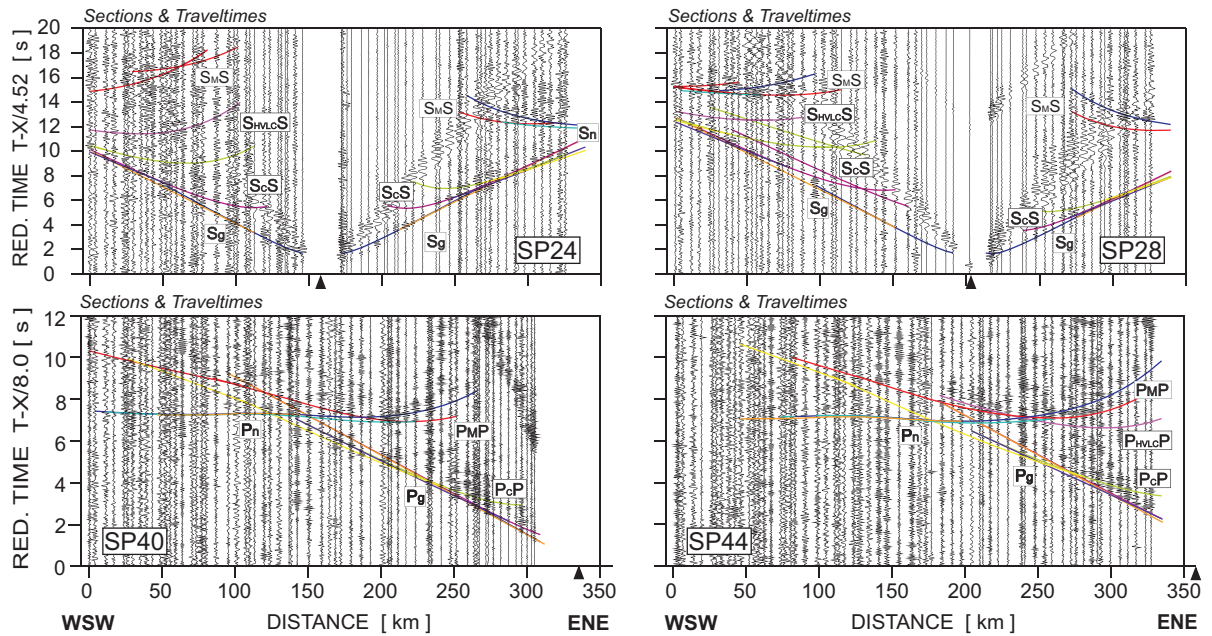


Figure 5. Quadruple plot of final model to real data fit with P- and S-wave, for shot points 40, 44 and 24, 28, respectively.

profiles such as regular WARR profiles FENNIA and BALTIC, and the low-cost profile KOKKY (Figure 1). The data about boundaries and velocities, which can be determined at the intersections of SOFIC profile with other profiles were interpolated to a starting model. An additional adverse circumstance is that intersections of these profiles with the SOFIC profile fall out at the ends of the profiles. As a result, the information we have, especially for deeper structures, derives from extrapolating the models to the locations of intersection.

The SEIS83 package (Červený & Pšenčík 1984) and graphical interfaces MODEL (Komminaho 1998) and ZPLOT (Zelt 1994) were used for forward modelling. The SEIS83 package was used to calculate ray paths, travel times, and synthetic seismograms seen in Figures 2-5. The final model was compiled using trial-and-error forward modelling. In the iterative process, travel times calculated for current velocity model were compared with observed, and corrected towards misfit minimization. Synthetic seismograms were calculated for qualitative control over modelled

and observed amplitudes, as done for the KOKKY profile. For a more detailed explanation of the procedure, see Tiira et al. (2020).

The two-dimensional forward modelling with ray tracing method resulted in P-wave velocity distribution model for SP01 and SP16 is visible in Figure 3. Starting with general geophysical assumptions, P-wave velocity model was converted into the S-wave model based on average V_p/V_s ratios for corresponding individual layers in the crossing profiles. Then, the velocity modelling in individual layers was performed iteratively, constraining the boundaries from P-wave model, until the least misfit of S-wave. Figures 4 and 5 give examples of the P- and S-wave modelling. Final values of V_p/V_s ratio are shown in Figure 6, and explosion sites in Figure 7.

3. Results

In our final crustal model, all velocities were gathered from previous profiles crossing the SOFIC

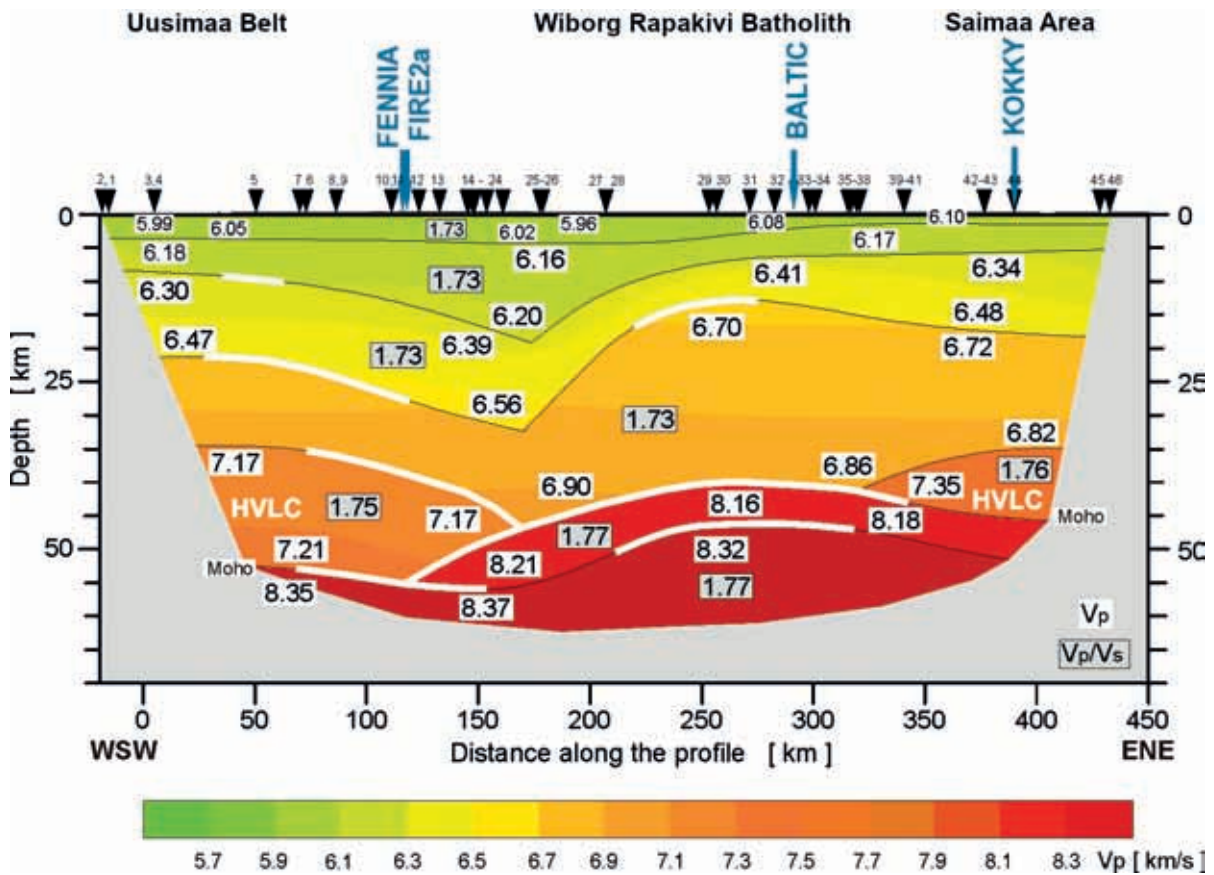


Figure 6. Final two-dimensional seismic model of P-wave velocity (V_p , boxes with white background) and distribution of V_p/V_s ratio (boxes with gray background). Confirmed boundaries are displayed with solid white lines. Numbered triangles indicate shot numbers. Crossing points of FENNIA, BALTIC, KOKKY and FIRE2a profiles are also shown. HVLC means the high velocity lower crust.

profile. Only fragments of model boundaries, which were obtained from the interpolation of data from intersecting profiles, were modified.

The modelling showed that P-wave velocities of 5.95–6.20 km/s characterized the uppermost rock layers. The depth range of these velocities increases from 0–8 km in the western part of the profile to ca. 0–15 km in the central part (ca. 170 km from the beginning) but decreases to 5 km near the eastern end of the profile. Two deeper crustal layers of the crust, middle crust with V_p ~6.3–6.56 km/s and a thickness of 7–15 km as well as lower crust with V_p ~6.7–6.9 km/s and a thickness of 15–25 km, repeat the geometry of the uppermost crust. They deepen and reach the boundary with the upper

mantle in central part of the model. There are high velocity lower crust (HVLC) layers at both ends, but not in the middle. The one at the western part (up to 150 km distance) has V_p ~7.2 km/s and a thickness of 15 km. The second one starts at 325 km from the beginning, has V_p ~7.35 km/s and reaches a thickness of ca. 10 km at the end of the profile.

Following the BALTIC model, two upper mantle layers were determined. The upper one with V_p ~8.2 km/s and a thickness of 7 km is present in all but the westernmost 125 km of the profile. The second deeper layer of V_p ~8.30–8.37 km/s extends along the entire profile. The Moho depth varies significantly, from ca. 52–54 km near the beginning of the profile to 40–43 km in the middle part and in

the end of the profile. V_p/V_s ratio generally remains closer to the range of 1.73 in the upper crust, but increases to 1.75–1.77 in the middle and lower crust and in the upper mantle.

Two-dimensional modelling only slightly changed the initial model. The initial information was based on the extrapolation of profiles intersecting with the SOFIC profile. Only boundaries with thick white lines (Figure 6) were verified by data from SOFIC. The ability to control the modelled structure decreases with the offset and the depth.

4. Discussion

4.1. Acquisition and data quality

At the time of carrying out the SOFIC fieldwork and the previous Kokkola-Kymi seismic survey (Tiira et al. 2019), there were few up-to-date and publicly available sources for verifying the shot locations. The interpretation of the seismic event origins was made on the basis of National Land Survey's topographic maps and aerial orthoimagery, satellite imagery contained in Google and Yandex's popular map services, information from regional news, and Finnish Transport Agency's public listings of road construction sites. Nowadays, there is a good availability of continuously updating optical and radar-based satellite remote sensing data, also known as Earth Observations (EO). For example, the Sentinel series of EU and ESA's Copernicus programme can provide observations of land cover and its changes at spatial resolutions as low as 10 meters, even several times a week (e.g. Phiri et al. 2020). At the time of SOFIC, the Operational Land Imager (OLI) onboard USGS Landsat-8 was one of the few high-resolution EO instruments whose data were publicly available, but its infrequent overpasses and a terrain resolution of 30 m did not allow us to consider it for this study.

The seismic sources registered during the recording were located at different distances from the profile, ranging from 0.23 km to 40.8 km.

The receivers did not cover the entire length of the profile, especially in its eastern end. The timing of events is probably less accurate than in KOKKY profile, since the survey line was set along the southern coast of Finland, and the azimuthal coverage of stations for locating events is low on the southern side. Quarry blasts are typically a series of several blasts with a certain time difference instead of one single explosion. This negatively affects the quality of the seismic signal. As a result, it was challenging to prepare an independent model such as in the case of KOKKY (Tiira et al. 2020). However, it was possible to control the consistency of data with earlier profiles.

4.2. Implications for geology

The previously established correlation of the WBR with mantle bulging, lack of HVLC, and overall thinner crust (Korja & Heikkinen 1995; Rämö & Haapala 2005) is visible in the crustal structure of the SOFIC profile as well. These features have been thought to reflect both compositional changes in the lower crust in response to partial melting caused by mantle-derived magmatism and mixtures of lower crustal and mantle material (e.g. Rämö & Haapala 2005). Regardless of the prevailing hypothesis that most of the Fennoscandian crust would be underlain by an enriched sub-continental mantle (e.g. Andersson 1984), these seismic observations also allow the earlier alternative interpretation based on isotopic evidence (Heinonen et al. 2010; 2015) that asthenospheric (depleted) mantle may have directly been involved in the genesis of the Wiborg rapakivi suite. Recent geobarometric results from the Wiborg suite anorthositic rocks also place the first crystallization stage of the rapakivi-related mantle-derived magmas at around 1.64 Ga in the depth of approximately 40 km and the last stages close to the surface (<7 km depth; Heinonen et al. 2020; Fred et al. 2020). Thus, the present-day Moho depth estimate for WRB from this study (40–45 km) conforms fairly well with the relative crystallization depths of the

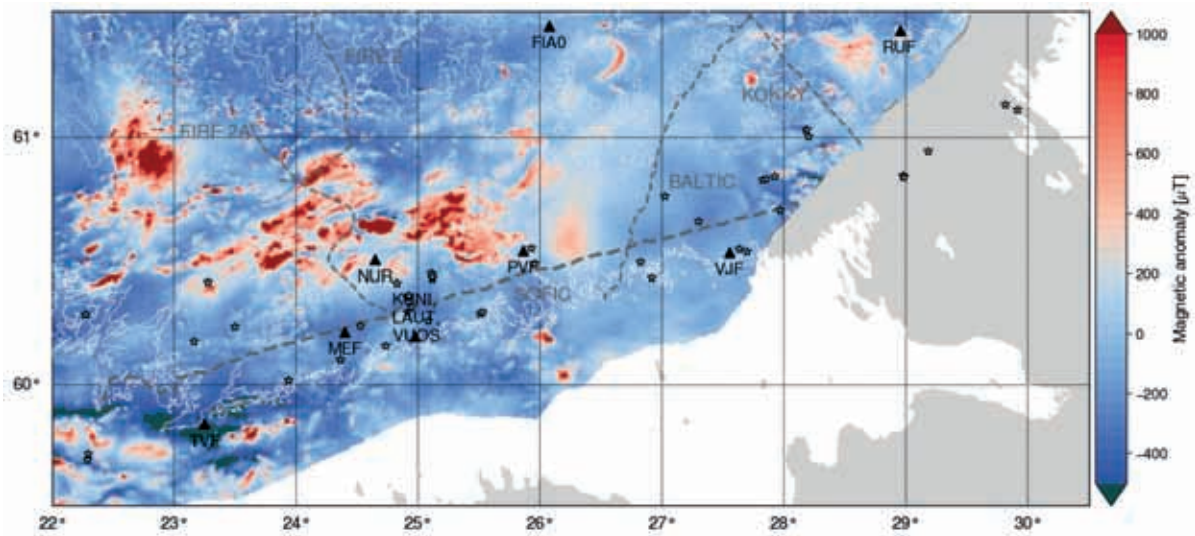


Figure 7. SOFIC profile (thick dashed line) and other deep seismic surveying profiles (thin dashed lines) in southern Finland plotted on an aeromagnetic anomaly map. Profile parts on the Russian territory are not shown. Star symbols show explosion sites, and triangle symbols denote permanent FNSN stations. Aeromagnetic data have been produced by the Geological Survey of Finland and can be downloaded at the Hakku service (<https://hakku.gtk.fi>, last accessed on the 4th of November, 2022).

rapakivi suite independently recorded by mineral geobarometry. The generally applied seismic cutoff depth associated with the transition from granitic to basaltic lithology at 350 °C in the Fennoscandian Shield (Veikkolainen et al. 2017) does not apply in the Wiborg suite where earthquakes are nonexistent below the depth of 5 km, thus raising a possibility of horizontal faults and fracture zones within the rapakivi block. Earthquakes in other areas of southern Finland are also typically shallow, but occasionally take place at greater depths such as the 7.6 km depth of an event on the 16th of December, 2020 in Raasepori (<https://www.helsinki.fi/fi/seismologian-instituutti/maanjaristykset-suomessa-2000-luvulla>, in Finnish, last accessed on the 4th of November, 2022), near the western end of the SOFIC profile. However, the rarity of events does not allow the determination of seismic cutoff depth.

The intersection of SOFIC and KOKKY profiles in the Russian Karelia also gives proof for shallow Moho assumption obtained from SOFIC. In addition, the deeper Moho at 170–325 km distance from the beginning of the profile is in agreement with FIRE2a (Figure 6). Even more

detailed information on the crustal structure can be obtained after the setup of HelsinkiNet (Veikkolainen et al. 2022). It is a collaborative seismological network maintained by the Institute of Seismology of the University of Helsinki, and owned by the City of Helsinki. However, all four HelsinkiNet stations KUNI, LAUT, RSUO and VUOS (Figure 7) are very close to each other and only supplement information from the national network and temporary deployments. They improve the location and time estimates for seismic events in the Helsinki region while the temporary seismic network in Kouvola area (Luhta et al. 2020) has facilitated the analysis of events in WRB and neighboring areas. To address increasing interests in studies of seismicity and lithospheric structure of WRB, two other seismic stations in WRB were established in Loviisa and Imatra in autumn 2021.

The SOFIC profile can be correlated with geophysical anomaly maps as well. The aeromagnetic data along the profile (Figure 7) are dominated by negative anomalies, except for an obvious positive anomaly at the boundary between UB and WRB. The northern boundary of WRB is

less distinct than the western one. Unfortunately, the full-resolution gravity anomaly map of Finland was unavailable for this study but it was possible to carry out a qualitative comparison of our results with the 3D density model of southern and central Finland (Kozlovskaya et al. 2004). The model of Kozlovskaya et al. (2004) showed no correlation between the Bouguer anomaly and Moho depth. This is contrary to the findings of the analysis of SOFIC. Below Uusimaa Belt, a 15 km thick HVLC is associated with a deep Moho. Below Saimaa Area, Moho is less deep, and the thickness of HVLC is merely 10 km, yet upper and lower boundaries of the lower crust are more uncertain here. On the other hand, Moho is most shallow below WRB, where no HVLC exists (Figure 6), and a negative Bouguer anomaly exists with sharply defined boundaries to the north and west. Data from the Russian side were unavailable and therefore geophysical contrasts of WRB to neighboring units in the east and south could not be determined.

5. Conclusions

The 450 km long SOFIC profile begins at 59.93° N, 22.41° E in Turku archipelago and ends at 60.96° N, 30.31° E south of Priozersk in Russian Karelia. The modelling shows that the Moho is deeper (52–54 km) in the Svecofennian lithosphere than below the Wiborg rapakivi batholith (40–45 km). Upper, middle, and lower crustal layers are well defined throughout the profile, and all have their maximum depths in the contact zone between the Svecofennian Uusimaa belt and the younger Wiborg rapakivi batholith. In the lower crust, P-wave velocity is only ~6.7–6.9 km/s below the rapakivi area and ~7.2 km/s below the Uusimaa belt. Below the Saimaa area, the value may be as much as ~7.35 km/s, but this value is uncertain due to the unfavorable event and station geometry. Unlike any other deep seismic sounding profiles in the shield, SOFIC runs in the direction similar to the E–W trending extensional regime in which the Wiborg batholith and other 1.65–1.62 Ga

rapakivi granites were formed in southeastern and southern Finland. However, the 1.59–1.54 Ga rapakivi granites in southwestern Finland are related to N–S extension (Nironen 1997). The location of SOFIC in the southernmost part of Finland, almost perpendicular to several other profiles, is important for the construction of a possible new 3D model of the Finnish lithosphere.

The outcome of the analysis supports the use of quarry blasts as a cost-effective reflection seismic source if the measurement geometry of portable geophones and permanent seismic stations is sufficient with not too large azimuthal gaps between the source and the receiver. It remains to be seen in future studies whether Earth Observations (EOs) from optical or radar instruments could complement the planning and execution of seismic surveys and provide independent means of verification for the shots' origins.

Acknowledgments

The analysis work essential for this paper was partially supported by a subsidy from the Polish Ministry of Education and Science for the Institute of Geophysics, Polish Academy of Sciences. We acknowledge the value of comments by Henning Lorenz, Suvi Heinonen, and an anonymous reviewer in improving the paper.

References

- Andersson, A.J., 1984. Geophysical interpretation of features in the marine geoid of Fennoscandia. *Marine Geophysical Researches* 7, 191–203. <https://doi.org/10.1007/BF00305420>
- Červený, V. & Pšenčík, I., 1984. Documentation of Earthquake Algorithms. In: Engdahl, E.R. (ed.) *SEIS83 - Numerical modeling of seismic wave fields in 2-D laterally varying layered structures by the ray method*. Report SE-35, Boulder, 36–40.
- Fred, R., Heinonen, A. & Heinonen, J.S., 2020. Equilibrium crystallization of massif-type anorthosite residual melts: a case study from the 1.64 Ga Ahvenisto complex,

- Southeastern Finland. *Contributions to Mineralogy and Petrology* 175, 86.
<https://doi.org/10.1007/s00410-020-01726-9>
- Havskov, J., & Ottemoller, L., 1999. SeisAn Earthquake Analysis Software. *Seismological Research Letters* 70, 532–534. <https://doi.org/10.1144/jgs2014-013>
- Heinonen, A.P., Andersen, T. & Rämö, O.T., 2010. Re-evaluation of Rapakivi Petrogenesis: Source Constraints from the Hf Isotope Composition of Zircon in the Rapakivi Granites and Associated Mafic Rocks of Southern Finland. *Journal of Petrology* 51, 1687–1709. <https://doi.org/10.1093/petrology/egq035>
- Heinonen, A., Andersen, T., Rämö, T. & Whitehouse, M.J., 2015. The source of Proterozoic anorthosite and rapakivi granite magmatism: evidence from combined in situ Hf-O isotopes of zircon in the Ahvenisto complex, southeastern Finland. *Journal of the Geological Society*, 172, 103–112. <https://doi.org/10.1144/jgs2014-013>
- Heinonen, A.P., Mänttari, I., Rämö, O.T., Andersen, T. & Larjamo, K.M., 2016. A priori evidence for zircon antecryst entrainment in megacrystic Proterozoic granites. *Geology* 44, 227–230.
<https://doi.org/10.1130/G37696.1>
- Heinonen, A.P., Rämö, T., Mänttari, I., Andersen, T. & Larjamo, K., 2017. Zircon as a Proxy for the Magmatic Evolution of Proterozoic Ferroan Granites; the Wiborg Rapakivi Granite Batholith, SE Finland. *Journal of Petrology* 58, 2493–2517.
<https://doi.org/10.1093/petrology/egy014>
- Heinonen A., Kivisaari, H. & Michallik, R.M., 2020. High-aluminum orthopyroxene megacrysts (HAOM) in the Ahvenisto complex, SE Finland and the polybaric crystallization of massif-type anorthosites. *Contributions to Mineralogy and Petrology* 175:10.
<https://doi.org/10.1007/s00410-019-1648-5>
- Hyvönen, T., Tiira, T., Korja, A., Heikkinen, P., Rautioaho, E. & SVEKALAPKO Seismic Tomography Working Group, 2007. A tomographic crustal velocity model of the central Fennoscandian shield. *Geophysical Journal International* 168, 1210–1226.
<https://doi.org/10.1111/j.1365-246X.2006.03242.x>
- Janik, T., 2010. Upper lithospheric structure in the central Fennoscandian shield: Constraints from P- and S-wave velocity models and v_p/v_s ratio distribution of the BALTIC wide-angle seismic profile. *Acta Geophysica* 58, 543–586. <https://doi.org/10.2478/s11600-010-0002-0>
- Janik, T., Kozlovskaya, E. & Yliniemi, J., 2007. Crust-mantle boundary in the central Fennoscandian shield: Constraints from wide-angle P and S wave velocity models and new results of reflection profiling in Finland. *Journal of Geophysical Research: Solid Earth*, 112, B4. <https://doi.org/10.1029/2006jb004681>
- Komminaho, K., 1998. Software Manual for Programs MODEL and XRAYs: A Graphical interface for SEIS83 Program Package. University of Oulu, Department of Geophysics, Report 20, 31 p.
- Korja, A., Korja, T., Luosto, U. & Heikkinen, P., 1993. Seismic and geoelectric evidence for collisional and extensional events in the Fennoscandian Shield – implications for Precambrian crustal evolution. *Tectonophysics* 219, 129–152. [https://doi.org/10.1016/0040-1951\(93\)90292-R](https://doi.org/10.1016/0040-1951(93)90292-R)
- Korja, A. & Heikkinen, P.J., 1995. Proterozoic extensional tectonics of the central Fennoscandian Shield: Results from the Baltic and Bothnian Echoes from the Lithosphere experiment. *Tectonics* 14, 504–517.
<https://doi.org/10.1029/94TC02905>
- Korja, A. & Heikkinen, P.J., 2008. Seismic images of Paleoproterozoic microplate boundaries in the Fennoscandian shield. In: Condie, K.C., Pease, V., (ed.) *When Did Plate Tectonics Begin on Planet Earth?* Geological Society of America Special Paper 440, 229–248. [https://doi.org/10.1130/2008.2440\(11\)](https://doi.org/10.1130/2008.2440(11))
- Kozlovskaya, E., Elo, S., Hjelt, S.-E., Yliniemi, J. & Pirttijärvi, M., 2004. 3-D density model of the crust of southern and central Finland obtained from joint interpretation of the SVEKALAPKO crustal P-wave velocity models and gravity data. *Geophysical Journal International* 158, 827–848.
<https://doi.org/10.1111/j.1365-246X.2004.02363.x>
- Kukkonen, I.T. & Lahtinen, R. (ed.) 2006. Finnish reflection experiment FIRE 2001–2005. Geological Survey of Finland, Special Paper, 247 p.
- Kurhila, M., 2011. Late Svecofennian leucogranites of southern Finland: Chronicles of and orogenic collapse. PhD thesis, University of Helsinki, Department of Geosciences and Geography A8, 105 p.
- Kähkönen, Y., 2005. Svecofennian supracrustal rocks. In: Lehtinen, M., Nurmi, P., Rämö, O.T. (ed.) *Precambrian Geology of Finland - Key to the Evolution of the Fennoscandian Shield*. Elsevier Science B.V., Amsterdam, 343–406.
[https://doi.org/10.1016/S0166-2635\(05\)80009-X](https://doi.org/10.1016/S0166-2635(05)80009-X)
- Lahtinen, R., Korja, A., & Nironen, M., 2005. Chapter 11. Paleoproterozoic tectonic evolution. In: Lehtinen, M., Nurmi, P. & Rämö, O.T. (ed.) *Precambrian Geology of Finland – Key to the Evolution of the Fennoscandian Shield*. Elsevier Science B.V., Amsterdam, 481–531. [https://doi.org/10.1016/S0166-2635\(05\)80012-X](https://doi.org/10.1016/S0166-2635(05)80012-X)
- Luhta, T., Komminaho, K., Oinonen, K., Tiira, T., Uski, M., Veikkolainen, T. & Vuorinen, T., 2020. Kouvola earthquake swarm - using a cross-correlator to find very small events and cluster them, EGU General Assembly 2020, Online, 4–8 May 2020, EGU2020-19417.
- Luosto, U., 1997. Structure of the Earth's crust in Fennoscandia as revealed from refraction and wide-angle reflection studies. *Geophysica* 33, 3–16.
- Luosto, U., Tiira, T., Korhonen H., Azbel, I., Burmin, V., Buyanov, A., Kosminskaya, I., Ionkis, V. & Sharov, N., 1990. Crust and upper mantle structure along the DSS Baltic profile in SE Finland. *Geophysical Journal International* 101, 89–110.
<https://doi.org/10.1111/j.1365-246X.1990.tb00760.x>

- Nironen, M., 1997. The Svecofennian Orogen: A tectonic model. *Precambrian Research* 86, 21–44.
[https://doi.org/10.1016/S0301-9268\(97\)00039-9](https://doi.org/10.1016/S0301-9268(97)00039-9)
- Nironen, M. (Ed.), 2017. Bedrock of Finland at the scale 1:1 000 000 - Major stratigraphic units, metamorphism and tectonic evolution. Geological Survey of Finland, Special Paper, 60, 128 p.
- Phiri, D., Simwanda, M., Salekin, S., Nyirenda, V.R., Murayama, Y. & Ranagalage, M., 2020. Sentinel-2 Data for Land Cover/Use Mapping: A Review. *Remote Sensing* 12, 2291. <https://doi.org/10.3390/rs12142291>
- Rämö, O.T. & Haapala, I., 2005. Chapter 12. Rapakivi Granites. In: Lehtinen, M., Nurmi, P., Rämö, O.T. (ed.) *Precambrian Geology of Finland - Key to the Evolution of the Fennoscandian Shield*. Elsevier Science B.V., Amsterdam, 533–562.
[https://doi.org/10.1016/S0166-2635\(05\)80013-1](https://doi.org/10.1016/S0166-2635(05)80013-1)
- Rämö, O.T., Turkki, V., Mänttari, I., Heinonen, A., Larjamo, K.M. & Lahaye, Y., 2014. Age and isotopic fingerprints of some plutonic rocks in the Wiborg rapakivi granite batholith with special reference to the dark wiborgite of the Ristisaari Island. *Bulletin of the Geological Society of Finland* 86 71–91.
<https://doi.org/10.17741/bgsf/86.2.002>
- Tiira, T., Janik, T., Skrzynik, T., Komminaho, K., Heinonen, A., Veikkolainen, T., Väkevä, S. & Korja, A., 2020. Full-Scale Crustal Interpretation of Kokkola–Kymi (KOKKY) Seismic Profile, Fennoscandian Shield. *Pure and Applied Geophysics* 177, 3775–3795.
<https://doi.org/10.1007/s00024-020-02459-3>
- Veikkolainen, T., Kortström, J., Vuorinen, T., Salmenperä, I., Luhta, T., Mäntyniemi, P. & Hillers, G., 2021. The Finnish National Seismic Network: Toward Fully Automated Analysis of Low-Magnitude Seismic Events. *Seismological Research Letters* 92, 1581–1591.
<https://doi.org/10.1785/0220200352>
- Veikkolainen, T., Oinonen, K., Vuorinen, T., Kortström, J., Mäntyniemi, P., Lindblom, P., Luhta, T., Hällsten, J., & Tiira, T., 2022. Helsingin seisminen asemaverkko ja seismisyys 2021. Institute of Seismology, University of Helsinki, Report T-106, 35 p. (in Finnish).
- Veikkolainen, T., Kukkonen, I.T. & Tiira, T., 2017. Heat flow, seismic cut-off depth and thermal modeling of the Fennoscandian Shield. *Geophysical Journal International* 211, 1414–1427. <https://doi.org/10.1093/gji/ggx373>
- Zelt, C.A., 1994. Software Package ZPLOT. Bullard Laboratories, University of Cambridge.